Specular and off-specular polarized neutron reflectometry of canted magnetic domains in loose spin coupled CuMn/Co multilayers

T. Saerbeck,[1,2,*] N. Loh,[1,2] D. Lott,[3] B. P. Toperverg,[4,5] A. M. Mulders,[2,6,7] M. Ali,[8] B. J. Hickey,[8] A. P. J. Stampfl,[2,9] F. Klose,[2] and R. L. Stamps[1,10]

[1]*School of Physics, University of Western Australia, Crawley, WA6009, Australia*
[2]*Australian Nuclear Science and Technology Organisation, Menai, NSW 2234, Australia*
[3]*Institute for Materials Research, Helmholtz Zentrum Geesthacht, D-21502 Geesthacht, Germany*
[4]*Department of Physics, Ruhr-University Bochum, D-44780 Bochum, Germany*
[5]*Petersburg Nuclear Physics Institute, 188300 Gatchina, Russia*
[6]*School of Physical, Environmental and Mathematical Sciences, UNSW in Canberra, ACT 2600, Australia*
[7]*Department of Imaging and Applied Physics, Curtin University of Technology, Perth, WA 6845, Australia*
[8]*School of Physics and Astronomy, University of Leeds, Leeds LS29JT, United Kingdom*
[9]*School of Chemistry, The University of Sydney, NSW 2006, Australia*
[10]*School of Physics and Astronomy (SUPA), University of Glasgow, Glasgow 612 8QQ, Scotland, United Kingdom*

(Received 18 September 2011; revised manuscript received 1 December 2011; published 17 January 2012)

Specular and off-specular polarized neutron reflectometry of strong biquadratic coupling in a $Cu_{0.94}Mn_{0.06}$/Co multilayer is presented. Detailed analysis of the reflectivity via the distorted-wave Born approximation reveals a formation of on average $\langle \pm 30^\circ \rangle$ canted lateral magnetic domains. Domains with mean width of 0.43 μm extend throughout the multilayer structure and magnetization alternates in the sign of the canting with subsequent layers. Temperature and field dependence of the magnetic structure are evaluated and included in the magnetic model, which is used to deduce bilinear and biquadratic interlayer exchange coupling energies.

DOI: 10.1103/PhysRevB.85.014411 PACS number(s): 75.70.Cn, 75.70.Kw

I. INTRODUCTION

Artificially created magnetic structures with confined length scales in the nanometer range are of ever-growing interest for scientific and technological reasons.[1] A particular field of interest, due to the prospect of a wide tuneability of physical properties to specific functionalities,[2] is magnetic multilayers (MLs) with magnetization of neighboring layers exchange coupled through nanoscale spacer layers.[3,4] In most cases, however, even small changes in structure or composition of the spacer material can lead to inherently different behavior. In contrast to a majority of previous studies on exchange interaction via nonmagnetic metals,[5,6] this paper focuses on the intriguing effect of dilute magnetic impurities within the spacer layer.

In the following we present results of the depth-resolved magnetometry of a $Cu_{0.94}Mn_{0.06}$/Co multilayer obtained from polarized neutron reflectometry (PNR). Doping of the nonmagnetic Cu spacer, within a Cu/Co multilayer, with low concentrations of Mn atoms has been shown by transport measurements to lead to noncollinear Co magnetization arrangements with a particular temperature dependence.[7] To date, however, no conclusive magnetic structure has been reported. In our recent report on dilute magnetic impurities in $Cu_{0.94}Mn_{0.06}$/Co multilayers we derive a theoretical description of a temperature-dependent biquadratic component, which is found to stabilize a noncollinear magnetic structure in the Co layer.[8] The theoretical model is based on experimental observations of in-plane correlated lateral domains, which have been observed with PNR. Here, we present the full description of the experimental study using the PNR technique and work out the details of the experimental data analysis and simulation. While the earlier report only focuses on two temperatures at low fields (300 K and 30 K at 7 mT), now a broad range of temperatures and external fields is presented. Additional structural measurements and complementary x-ray scattering give further information on the interpretation of the data. A comprehensive model of the three-dimensional (3D) magnetic structure at each temperature and external field is derived, based on fitting and simulation of the experimental data, which is described in detail. A discussion of the results makes use of the determined domain structure, coupling angle, and external field dependence to derive bilinear and biquadratic exchange coupling energies, which are compared to the theoretical model presented earlier.[8] The sample structure under investigation consists of 30 repetitions of a [$Cu_{0.94}Mn_{0.06}$(19Å)/Co(21Å)] bilayer, which exhibits a Cu-mediated Ruderman-Kittel-Kasuya-Yosida (RKKY) interaction comparable in strength to the magnetic coupling originating from the Mn impurities. Investigations on different spacer layer thicknesses within the range of strong biquadratic coupling[7] reveal a consistent behavior of exchange coupling parameters, thus indicating a phenomenon of greater generality rather than well-matched coupling terms.

In Sec. II we will give a brief introduction of the PNR experiment, while more detailed theoretical considerations are made in the corresponding section containing the analysis. Section III describes the analysis of specular reflectivity (Sec. III A) and off-specular scattering (Sec. III B), as well as the magnetic field and temperature dependence (Sec. III C). In the discussion, Sec. IV, experimental exchange coupling energies are derived and we conclude in Sec. V.

II. EXPERIMENT

Polarized neutron reflectometry enables a quantitative, depth-resolved determination of magnitudes and directions of magnetization vectors in thin layers of subnanometer to μm length scales.[9] Depth and laterally resolved magnetic models

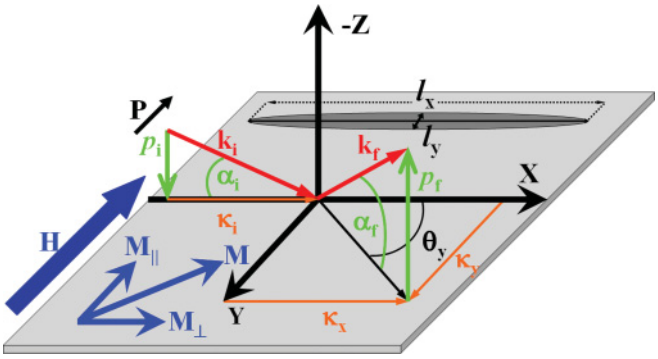

FIG. 1. (Color online) General schematic of neutrons being reflected from a surface. p_i and κ_i are the vertical and longitudinal projections of the incoming wave vector k_i of the neutrons, while p_f, κ_x and κ_y denote the corresponding projections of the outgoing wave vector k_f. H is the external field direction. The gray shaded area in the upper part of the figure illustrates the shape of the neutron coherence area, which is described in the discussion of the off-specular scattering.

can be inferred from spin resolved specular and off-specular scattering via simulations of 2D reflectivity profiles as a function of temperature and external magnetic fields. The model parameters, arising from the fitting of specular PNR and simulations of off-specular scattering performed with specially developed software,[10] are shown to contain enough information to form the basis for a detailed theoretical description of the temperature-dependent biquadratic coupling.

Experimentally, a collimated, spin polarized neutron beam is impinging onto the sample surface under a shallow incident angle α_i (Fig. 1). The wave vector $k_i = 2\pi/\lambda$ of the incoming neutrons can be decomposed into an in-plane component κ_i and an out-of-plane component p_i. Neutrons interact with the sample, and are scattered under a glancing outgoing angle α_f with a final moment k_f, which consists of the projections κ_x, κ_y, and p_f. In our PNR geometry, scattering along the y direction is not resolved due to a relaxed collimation $\Delta\theta_y$ along the corresponding angle of θ_y and thus the scattering cross section is integrated over the wave vector transfer projection κ_y.[11] The neutron polarization vector P is directed by the external field H to lie within the plane of the sample perpendicular to the neutron propagation direction.

The PNR measurements have been performed using the neutron reflectometer NERO, which operates in the angular dispersive mode with constant wavelength $\lambda = 4.33$ Å at the Helmholtz Zentrum Geesthacht (formerly GKSS), Germany.[12] The instrument is equipped with a transmission-type supermirror polarizer for the incident beam, a pair of Mezei-type spin flippers, and a multichannel analyzer[13] discriminating spin states of neutrons scattered into a broad range of wave vector transfers recorded over the 2D position sensitive detector (PSD). A combined polarization efficiency of the polarizer and the analyzer of ~97%, was determined experimentally and verified by simulations presented in this paper. The setup allows for simultaneous spin-dependent detection of specular and off-specular scattering events. The magnetic structure manifests itself in the neutron reflectivity via differences in the detected spin channels R^{++}, R^{--}, R^{+-}, and R^{-+}, where the superscript denotes the direction of the incoming (first superscript) and reflected (second superscript) neutron polarization as parallel (+) or antiparallel (−) with respect to the external guide field direction. The two non-spin-flip (NSF) reflectivities R^{++} and R^{--} arise from nuclear and magnetic scattering potential contrast at interfaces, due to projections $M_{||}$ of the magnetization M parallel to the neutron spin. Spin-flip reflectivities R^{+-} and R^{-+} on the other hand are exclusively due to the component $M_\perp$ of the magnetization vector perpendicular to the vector of the incident neutron polarization.

A 1 T electromagnet at the sample position and a 30 K closed-cycle refrigerator are used to establish sample environment conditions. Prior to each measurement a saturating field ($H = 600$ mT) applied in the plane of the sample ensures equivalent conditions and magnetic history of the sample. If not stated otherwise, a $H = 7$ mT guide field was applied in the same direction during the measurements, needed along the neutron path to maintain the polarization of the neutrons.

III. RESULTS

A. Specular reflectivity

Specularly reflected intensities obey an energy and in-plane momentum conservation law, with $\kappa_i = \kappa_x$ and, consequently, for purely elastic reflection $\alpha_i = \alpha_f$ (Fig. 1). This leads to a wave vector transfer

$$Q_Z = 2p_i = \frac{2\pi}{\lambda}[\sin(\alpha_i) + \sin(\alpha_f)], \tag{1}$$

due to the neutron interaction described via a 1D potential

$$V = \frac{2\pi\hbar^2}{m_n}(\varrho^n \pm \varrho^m) = \frac{2\pi\hbar^2}{m_n}Nb_n \pm B \cdot s, \tag{2}$$

in which $\varrho^n = Nb_n$ describes the nuclear scattering length density (SLD) with an atomic density N and coherent scattering length b_n of the material (for recent reviews on PNR see Refs. 14 and 15). m_n denotes the neutron mass. The second term, ϱ^m, describes the interaction between the neutron magnetic moment associated with the operator s, whose Cartesian components are proportional to Pauli spin matrices[11,15] and the magnetic induction B created by the magnetic moments of the sample. In a simple approach, specular reflectivities can be calculated in a standard Fresnel theory by solving the stationary spin-dependent Schrödinger equation and matching the spin components of the neutron wave function inside and outside the medium.

The top profile of Fig. 2 shows the spin-dependent specular reflectivity of the multilayer at 30 K with the Co layers saturated by an external magnetic field of 560 mT. To enhance the statistical accuracy and to account for the broadening of the specular beam on the detector, the profile shown is obtained by an integration of the intensity on the area detector over a region of 0.25° around the actual specular ridge with $\alpha_i = \alpha_f$. The plot of experiment and fit therefore include resolution effects that broaden the beam. Kiessig fringes, observed along the decay of the reflectivity below $Q_Z = 0.05$ Å^{-1}, are the result of an enhanced resolution in this measurement. Periodicities of the oscillations confirm the total thickness of the sample. In all other respects, the data reproduces the reflectivity of the sample in its remanent state at 300 K.[8] The difference in the critical

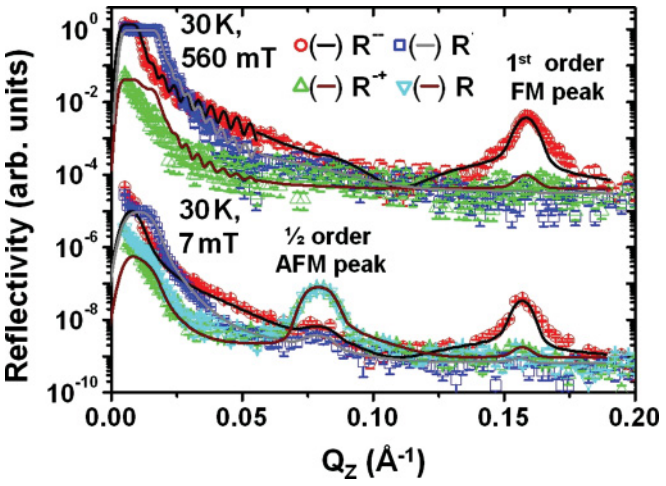

FIG. 2. (Color online) Normalized specular polarized neutron reflectivities at 30 K of the sample in a magnetically saturated state in $H = 560$ mT (top profile) and canted state at 30 K in 7 mT external field (bottom profile, reproduced from Ref. 8) in – – (red circles), ++ (blue squares), +– (cyan triangles), and –+ (green triangles) polarization. Lines are fits to the data (Ref. 10). Individual datasets have been offset by four orders of magnitude for clarity reasons.

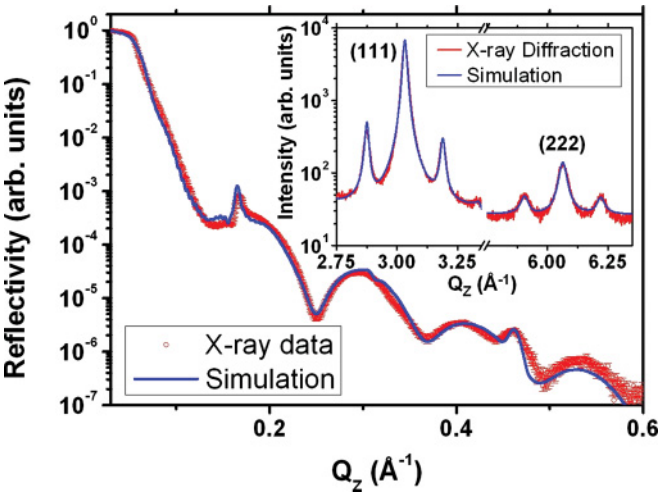

FIG. 3. (Color online) X-ray reflectivity at 300 K recorded with Cu K_α radiation. The simulations have been performed using the program SIMULREFLEC (Ref. 20). Inset: High-angle x-ray diffraction showing the (111) and (222) lattice peaks and first-order satellites on either side corresponding to the multilayer periodicity [simulations performed with SUPREX (Ref. 17)].

wave numbers for total reflection, $Q_{Z,c} = \sqrt{16\pi(\varrho^n \pm \varrho^m)}$, of neutrons with alternative polarization directions immediately provides the averaged magnetic moment, which has been determined to $m_{Co} = 1.46\ \mu_B$/atom, corresponding to 85% of the literature value.[16] This averaged moment leads to a combined nuclear and structural scattering length density of Co of $\varrho_{Co}^{n+m} = 5.77\ \text{Å}^{-2}$, which is comparable to the nuclear SLD of Cu ($\varrho_{Cu}^{n} = 5.96\ \text{Å}^{-2}$) and providing a very small scattering contrast for the R^{++} channel. The bilayer periodicity therefore only leads to a sufficient contrast in the R^{--} channel, giving rise to a first-order Bragg peak, which is a direct indication of a collinear alignment of subsequent Co magnetizations. The Q_Z position of the first-order Bragg peak, $Q_{Z,\text{Bragg}} \approx \sqrt{Q_{Z,c}^2 + (2\pi\Lambda)^2}$ corresponds to a bilayer periodicity of $\Lambda = 40$ Å. The detected SF signals are solely due to limited polarization efficiencies of the polarizer, analyzer, and spin flippers, allowing admixture of 3% NSF signal to SF channels and vice versa. This admixture is taken into account via fitting of all four channels simultaneously.[10] Corefinement with complementary x-ray reflectometry and high-angle x-ray diffraction (Fig. 3), gives a structural model of the ML (Fig. 4). The high-angle x-ray diffraction (Fig. 3, inset) confirms the coherent growth of the multilayer with a pronounced (111) texture (lattice constant $a = 3.61$ Å). First-order satellites of the center (111) peak arise from the superlattice periodicity of $\Lambda = 40$ Å, simulated[17] in agreement with reflectometry results (Fig. 3). Using the full-width-half-maximum (FWHM) of the (111) peak in the Scherrer formula with a Scherrer constant of $K = 0.94$,[18,19] gives an average coherence length of 200 Å along the direction normal to the sample surface. With respect to the periodic layer structure, the average coherence length therefore approximates to five times the $Cu_{0.94}Mn_{0.06}$/Co bilayer periodicity. Figure 4 shows depth profiles of the x-ray and neutron reflectometry deduced scattering length densities. The total thickness of the sample and individual thicknesses of each layer are in agreement within 5% with the nominal sample structure. Densities of each material, used to calculate the SLD, are taken from the bulk literature values. The reflectometry fit of both x-ray (using SIMULREFLEC)[20] and PNR (Figs. 2 and 3) resulted in a combined structural and magnetic roughness of 9 Å, averaged over the multilayer stack. The top four bilayers of the multilayer stack have been treated separately from the rest of the periodic structure to allow for larger variations in layer thickness and roughness increasing toward the multilayer surface. In addition, PNR and x-ray fits have not been restricted to the same parameter set, but allowed for a variation of the top four bilayer parameters between the different techniques. This treatment of both fitting procedures is sufficient to account for experimental and sensitivity differences x-ray and neutron reflectometry and a very good agreement of parameters is

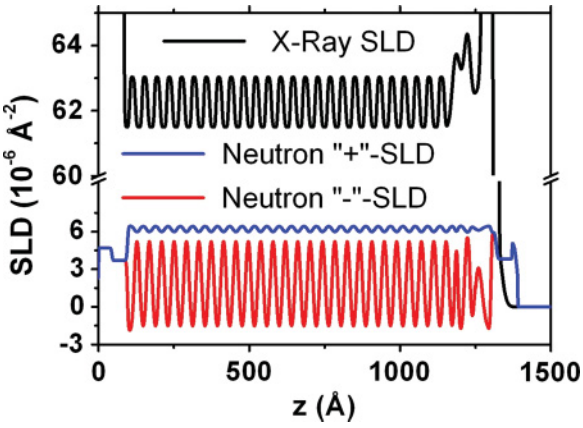

FIG. 4. (Color online) Scattering length density profiles applied in the x-ray and neutron reflectometry simulations. The multilayer part has been simulated with an averaged roughness of 9 Å and the top four bilayers adjusted to account for increased roughness and waviness closer to the multilayer surface.

found for the remaining, main part of the multilayer. While the x-ray SLD profile at 300 K displays the nuclear only structure of the sample, the neutron SLD profile contains the magnetic information of the sample in its saturated state. The high agreement between the low-temperature saturated and the 300 K remanent state proves the FM-type alignment of Co magnetizations at high temperatures in zero or low magnetic fields (7 mT guide field).[8] In addition, the similarity of the two measurements shows the validity of a structural model unvarying with temperature, which can therefore be used in all following simulations.

As identified by Saerbeck *et al.*[8] the low-temperature reflectivity profile at 30 K without the saturating field exhibits an additional peak of purely magnetic origin (Fig. 2, bottom). The half-order position of this peak with respect to the first-order Bragg peak identifies an antiferromagnetic alignment of subsequent layers, while the SF nature of the signal indicates a canting of the magnetization.[11,21] Regarding the analysis via fitting and simulation of the AFM half-order peak, which represents the central dataset for observation of the temperature-dependent coupling,[8] we now turn to the full 2D reflectivity profile, including off-specular scattering components.

B. Off-specular scattering

The 2D detector image of the SF half order peak,[8] shows a strong diffuse off-specular scattering (Fig. 5). The data on specular and off-specular scattering are collected into the scattering map displayed in the left column of the contour plots in Fig. 5(a), in Q_X/Q_Z coordinates, where

$$Q_X = \frac{2\pi}{\lambda}[\cos(\alpha_f) - \cos(\alpha_i)], \tag{3}$$

is the lateral wave vector transfer. The corresponding simulated map of the SF scattering is shown in the right column in the same coordinates. In order to provide a quantitative comparison between experimental data and simulation, off-specular scattering profiles from all reflectivity channels [Fig. 5(c)] have been obtained by integrating a 0.01Å^{-1} wide region around the center AFM peak location at $Q_Z = 0.08$ Å^{-1}.

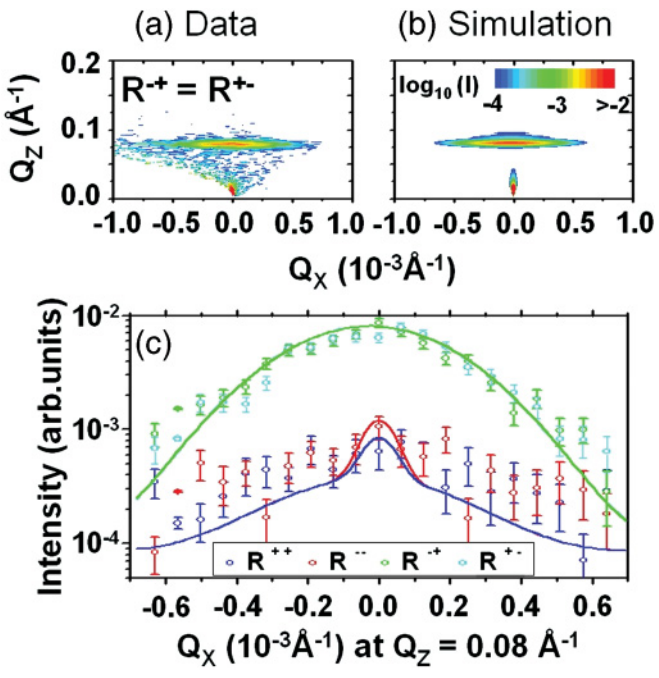

FIG. 5. (Color online) (a) Off-specular Q_X/Q_Z scattering profiles of NSF and SF channels with $R^{+-} = R^{-+}$ and corresponding simulations (Ref. 8) (b) The color scale is adjusted to enhance visibility of off-specular features and limited to $I \leqslant 10^{-2}$. (c) Off-specular peak profile along Q_X taken at a constant $Q_Z = 0.08$ Å.

Off-specular scattering originates from lateral structures that break the in-plane translational symmetry of the sample and lead to an in-plane momentum transfer $Q_X = \kappa_i - \kappa_x \neq 0$. Violation of the lateral translation invariance may originate from structural and magnetic lateral defects, such as interfacial roughness and magnetic domains. The fact that off-specular scattering is mostly detected in the SF channel[8] justifies a magnetic source of the scattering (e.g., magnetic domains whose magnetization is not collinear with the polarization).

Note, that due to the birefringence effect, off-specular SF scattering is an asymmetric function of Q_X in a partially magnetized sample and R^{-+} is not identical to R^{+-} along Q_X, but rather mirrored at $Q_X = 0$ [$R^{-+}(+Q_X) = R^{+-}(-Q_X)$].[21–24] The asymmetry in R^{-+} and R^{+-} is, however, mostly expressed in the range close to the total reflection of incoming or scattered neutron waves, while being hardly visible in the Q_X/Q_Z representation with reduced view on small Q_Z. Therefore, in Fig. 5, only R^{-+} is depicted and discussed here as being equal to R^{+-}.

The SF scattering maps (Fig. 5) demonstrate that the AFM peak in Fig. 2 is in fact of purely off-specular origin due to scattering from magnetic domains within the plane of the sample and no true specular SF reflection contribution is detected at $\alpha_i = \alpha_f$.

The treatment of off-specular scattering has only recently found extensive consideration via the distorted-wave Born approximation (DWBA), in which lateral structures represent a small perturbation to the smooth surface or interface.[11,25] One first evaluates the exact wave functions for the neutrons interacting with the mean film potential, averaged over the lateral coordinate. The second step is a perturbation calculation using these derived wave functions and the perturbation potential, which is the difference between the actual potential and its mean value. In case of lateral magnetic domains, the perturbation potential is given by the lateral fluctuation of the magnetic moment,[22] while the magnetic scattering operator is given by the domain form factor.[23] Therefore, for a complete description of the magnetic structure, the averaged mean layer magnetization M and individual domain magnetizations m have to be considered. A more detailed theoretical description of off-specular scattering and the simulation routine, which is based on the supermatrix formalism,[24,26] or super-recursion formalism[11] can be found in the references cited above.

Phenomenologically, the diffuse off-specular scattering can be described as a type of coherent scattering from magnetic domains in the plane of the sample.[27] In order to fulfill the coherent scattering condition, domains need to be smaller than the 3D neutron coherence volume projected onto the sample

surface. This area can be estimated via the uncertainty in momentum transfer ΔQ_X and ΔQ_Y in the corresponding in-plane directions. Such an uncertainty is a direct consequence of the angular divergence $\Delta\alpha_i$, $\Delta\alpha_f$, and $\Delta\theta_y$, due to the neutron beam collimation used during the experiment[11]

$$\frac{1}{l_x} \sim \Delta Q_x \sim \frac{\pi}{\lambda}\sqrt{(\alpha_i \Delta\alpha_i)^2 + (\alpha_f \Delta\alpha_f)^2}, \quad (4)$$

$$\frac{1}{l_y} \sim \Delta Q_y \sim \frac{\pi}{\lambda}\Delta\theta_y \gg \Delta Q_X. \quad (5)$$

The slit system of NERO was set up to a 0.95 mm neutron beam with a divergence of 0.037° in the x direction, while no collimation in the y direction is applied. The neutron coherence volume therefore comprises a cigar-shaped area of about $l_X \sim 42$ μm along the long axis and only a few 10 Å along the perpendicular direction l_y (see sketch Fig. 1). Shape and intensity of the diffuse scattering along Q_Z and Q_X are determined by the size distribution of domains and individual magnetic structure. The width of the scattering along Q_Z is described by a replication factor in depth, defining the length scale over which a particular domain structure is repeated in the multilayer. For our case, it was found to be reproduced in depth throughout the stack, since the specular reflected first-order Bragg peak shows a similar broadening due to thickness fluctuations and roughness. Furthermore, the diffuse scattering is concentrated around the half-order position and no evidence of scattering from vertically uncorrelated regions, evenly distributed in Q_Z,[28] has been observed. Due to the experimental geometry, approaching the direct neutron beam at $Q_Z = 0$ results in an increase in detected background intensities [Fig. 5(a)]. The simulations, on the other hand, only include a constant background at the lower limit of the color scale in Fig. 5(b).

The profile along the off-specular direction Q_X is described via a formalism in analogy to neutron small angle scattering with an in-plane correlation function describing the magnetic domain form factor,

$$\langle|\Delta m(Q_X)|^2\rangle = \frac{\langle|\Delta m|^2\rangle\xi}{\sqrt{2\pi}} \exp\left(-\frac{Q_X^2\xi^2}{2}\right), \quad (6)$$

averaged over the domain size distribution. Here, no correlations between domain sizes and directions of magnetizations are assumed. Therefore, $\langle|\Delta m|^2\rangle$ describes the mean square of the in-plane projections of adjacent domain magnetizations onto the X direction, and the parameter ξ, in accordance with the Guinier approximation,[29] refers to the in-plane gyration radius of domains. Note that in general, averaged over Gaussian size distribution, the domain form factor should be described by a modified Voigt function decaying at large Q_X as a power law. However, due to the restricted dynamical range of our measurements, only the Guinier region of Q_X was accessible. In this region, a Voigt function can be represented by the Gaussian function (6), which is sufficient to describe our data, varying only two parameters $\langle|\Delta m|^2\rangle$ and ξ. This was performed under the condition of absolute normalization of the off-specular scattering intensity to the specularly reflected intensity. The best fit to the data was achieved with an average domain size of $\xi = 0.43$ μm. A possible explanation of the average domain size can be connected to the average in-plane crystallite size of the highly textured film. While the out-of-plane x-ray diffraction gives an average coherence length of 0.2 μm, it is well possible that the average crystallite size is much larger. In addition, the in-plane crystalline structure is expected to be different to the degree of texture found along the growth direction of the sample.

Domains larger than the coherence length do not contribute to off-specular scattering, but affect specular intensities via an incoherent summation of reflectivities from different domains (>42 μm) on different locations of the sample area. With smaller domain sizes, the coherence volume covers more and more domains and neutrons are reflected specularly from the mean magnetization $\langle M\rangle$ averaged over the domains crossed by the coherence ellipsoid. The direction of $\langle M\rangle$ is described by an angle γ with respect to the neutron polarization. Deviations of the domain magnetization m from the mean magnetization $\langle M\rangle$, characterized by the canting angle $\Delta\gamma$, cause NSF and SF off-specular scattering. The SF scattering therefore probes fluctuations transverse to $\langle M\rangle$ and provides information of individual domain magnetizations and magnetic roughness. In the Q_X/Q_Z scattering maps (Fig. 5) the off-specular scattered intensity is restricted to the spin-flip channels R^{-+} and R^{+-}, which points to a canted domain magnetization in the Co layers (Fig. 6). The absence of NSF off-specular scattering[8] illustrates that the canting of individual domains $\pm\Delta\gamma$ points symmetrically to the left and right of the mean magnetization

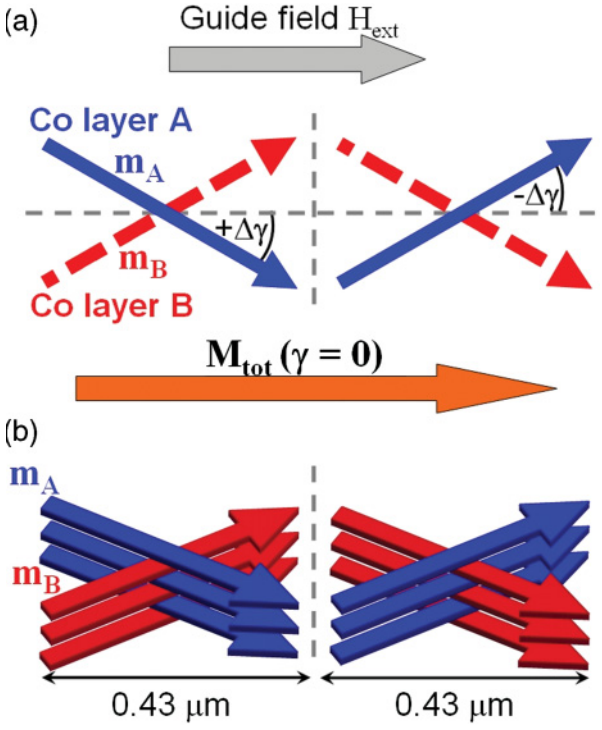

FIG. 6. (Color online) Schematic of the magnetic structure in the multilayer at 30 K with 7 mT external guide field. (a) Top view of two adjacent domains with two subsequent Co magnetizations m_A and m_B, tilted by the angle $+\Delta\gamma = +30°$ and $-\Delta\gamma = -30°$, respectively. The averaged magnetization M_{tot} lies parallel to the guide field direction. (b) Perspective view of six subsequent domain configurations stacked columnlike in 0.43 μm domains throughout the multilayer.

⟨M⟩. This mean magnetization averaged across domains does not show appreciable deviations from the axis of the neutron spin ($\gamma = 0$, Fig. 6), as it can be seen from the vanishing SF specular reflectivity. It shall be noted that the sense of canting in each domain with respect to the mean magnetization is not uniquely determined by the performed experiments as only the averaged projection $\langle \sin^2(\Delta\gamma) \rangle$ is probed.[11] In order to obtain the complete 2D directional information on the source of scattering, one would need to obtain additional measurements with neutron polarization vectors perpendicular to the mean magnetization. In our case however, the essential information is already included in the 1D measurement and the required additional instrumentation is beyond the scope of this work.

In order to reproduce the spin-flip scattering with an AFM periodicity, the angle $\Delta\gamma$ has to alternate in sign with equal magnitude in subsequent Co layers A and B as well as laterally across the domains (Fig. 6). Because the mean magnetization direction is defined by the external field direction H, this leaves two options for domain configurations in each layer, which are schematically presented in Fig. 6. Simulations of the magnetic configuration at 30 K in 7 mT (Fig. 5) gave the best match to the data with a domain magnetization m canted by $\Delta\gamma_{A,B}(30\,K, 7\,\mathrm{mT}) = \pm 30^\circ$ in individual domains and in subsequent layers (Fig. 6). Thus, the domain magnetization in each pair of Co layers encloses an angle of $2\Delta\gamma = \Delta\gamma_A - \Delta\gamma_B = 60^\circ$. It has to be noted that the canting of small domains also affects magnetic scattering potentials via an effective reduction of the magnetic scattering length density by the factor $\cos(\Delta\gamma)$ relative to its saturation value, which is equivalent to a reduction in magnetization and in good agreement with magnetometry results.

C. Temperature and field dependence

After the discussion of a model for the remanent magnetization at 300 K ($\Delta\gamma = 0$, ferromagnetic alignment) and 30 K ($\Delta\gamma = 30^\circ$ canted structure), it is of interest to study the field and temperature behavior in more detail. For this purpose, temperature- and field-dependent PNR measurements have been performed and the magnetic structure evaluated for each experimental condition. Since the off-specular scattering is purely of magnetic origin and no NSF off-specular scattering has been detected, the following discussion shall be confined to observations in the SF channel only. All reported measurements, however, have been performed measuring all three relevant channels, R^{++}, R^{--} and R^{+-} and simulated consistently for each polarization with the structural model presented above. This approach guarantees correct scaling of relative intensities and averaged magnetizations. Additionally, the constant first-order Bragg peak observed with applied field disproves magnetic roughness as a possible cause for the off-specular scattering.[30,31]

Figure 7 shows the field dependence of the off-specular scattering at 30 K as Q_X/Q_Z scattering maps and line profile scans along Q_X for R^{-+}. For field values other than 7 mT, the low Q_Z intensity, resulting purely from polarization deficiency, is omitted. The peak profiles, shown in Fig. 7(b), indicate that the relative width of the off-specular peak profile stays constant with the increasing magnetic field. Simulations of each state gave the best match using the same 0.43 μm

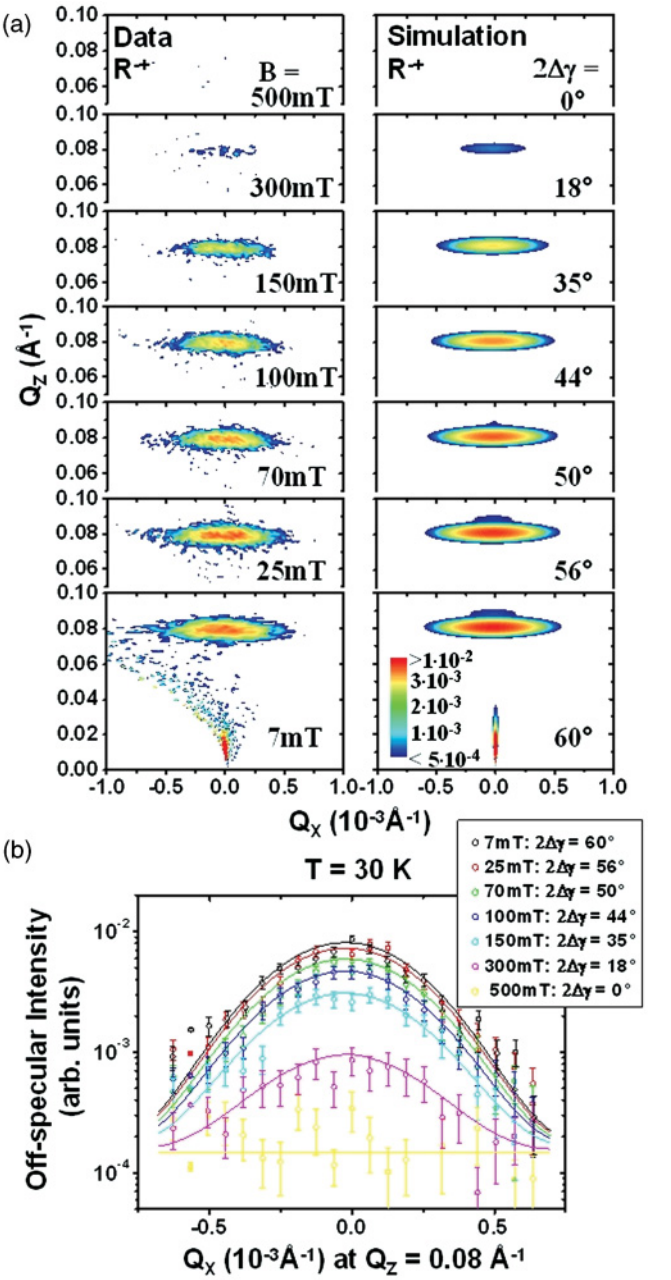

FIG. 7. (Color online) (a) Field dependence of off-specular R^{-+} scattering at 30 K from 0 mT to 500 mT. At a field of 500 mT, the scattering has become too weak to be detected. (b) Off-specular peak profiles along Q_X for various fields taken from line scans through the off-specular scattering maps at $Q_Z = 0.08 \pm 0.01$ Å^{-1} in (a).

domain width, but gradually closing magnetization vectors. In fact, the small domain magnetization angle $\Delta\gamma$ was the only parameter varied between the simulations and all other parameters, such as resolution, mean magnetization direction, and structural parameters had to remain fixed to achieve a consistent match to the data. Simulations of the peak at each field value show that the coupling angle is steadily decreasing with increasing field until no AF off-specular scattering is detectable at 500 mT. At this stage the projection onto the axis of the magnetization perpendicular to the neutron polarization has become too small to be detected. Magnetic realignment due

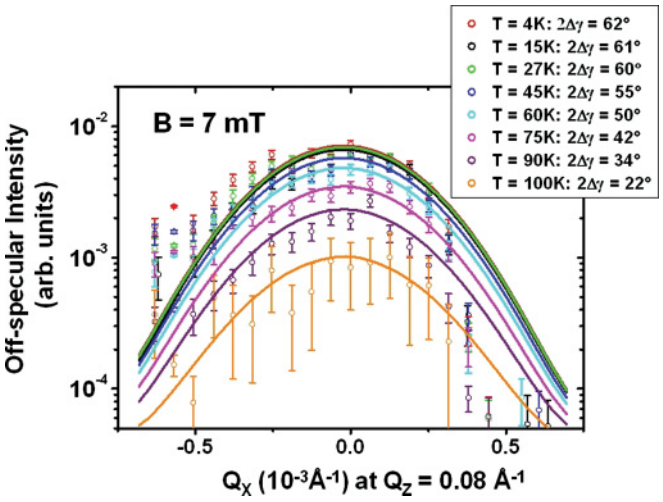

FIG. 8. (Color online) Off-specular peak profiles along Q_X at various temperatures taken from line scans through the off-specular scattering maps at the AF peak position $Q_Z = 0.08\ ^{-1}$.

to domain wall movement would lead to changes in the domain size, which is not observed due to the constant off-specular peak shape. The gradual rotation of magnetization vectors also does not lead to changes in the specular reflectivity or first-order Bragg peak, which is in agreement with the experiment. The field dependence of the coupling angle has been additionally determined at an increased temperature of 70 K.

Regarding temperature dependence of the interlayer exchange coupling, two experimental conditions are of main interest. The first parameter to be analyzed is the behavior of the coupling angle $2\Delta\gamma$ in remanent or low external field with respect to temperature. An evaluation of this is again performed by recording full 2D reflectivity profiles and analysis of the scattering via simulations adjusting only the domain canting angle $\Delta\gamma$. Figure 8 shows the off-specular peak profiles of the R^{-+} polarization channel in 7 mT external field. Note, that the asymmetric shape of the data in Fig. 8 resulted from shadowing by a beam stop, inserted to block the direct neutron beam and reduce background scattering during the measurement. The beam stop was removed for all other measurements. In the simulations determining the gradually closing coupling angle, regions of suppressed intensity have been omitted and a constant domain width was assumed based on the data not influenced by the beam stop. Above 100 K no AF intensity is observed, which indicates the onset temperature of the canted magnetization in each layer. No changes, apart from an increase in total magnetization, in the R^{++} and R^{--} specular reflectivities are observed (Fig. 2).

The second parameter of interest is the external field strength needed to overcome the coupling and saturate the magnetic structure.[8] The information about this saturating field H_S has be obtained by recording the half-order peak intensity of the AF peak at different temperatures versus external in-plane field. As the general field dependence at 30 K indicates, magnetization vectors rotate gradually into the direction of the external field and a vanishing half-order signal can be interpreted as a collinear alignment of magnetizations, which resembles a saturated state.

TABLE I. Comparison of exchange coupling parameters for different $Cu_{0.94}Mn_{0.06}$ thicknesses t_{CuMn} at $T = 30$ K in $H = 7$ mT external guide field.

t_{CuMn} (Å)	Coupling Angle $\Delta\gamma$ (°)	Domain Width ξ (μm)	Depth Replication (Number of bilayers)
16	23	0.40	30
19	30	0.43	30
25	29	0.35	8

IV. DISCUSSION

A comparison of magnetization structures evaluated for different $Cu_{0.94}Mn_{0.06}$ spacer layer thicknesses t_{CuMn}, such as the coupling angle $\Delta\gamma$, the lateral magnetic domain width ξ and the replication of the canted structure in depth, is summarized in Table I. The magnetic replication factor, given in numbers of the bilayer structure $Cu_{0.94}Mn_{0.06}$/Co, measures the amount of layers throughout which the canted structure is coherently reproduced. Parameters listed in the table represent the coupling state at 30 K in the low 7 mT magnetic guide field and have been consistently analyzed with the procedure presented above. Coupling angles and lateral domain width are found to be consistent within the investigated thickness range, which is in agreement with the thickness-dependent coupling behavior as evaluated by magnetoresistive measurements.[7] The sample with 25 Å $Cu_{0.94}Mn_{0.06}$ shows a depth replication factor reduced to eight bilayer repetitions, consistent with a decrease of the overall exchange coupling strength with thicker spacer layer thickness.

Figure 9(a) shows a summary of the magnetic coupling angle versus field for the sample with 19 Å $Cu_{0.94}Mn_{0.06}$, which is used as a basis for a theoretical modeling in connection with the temperature dependence of the coupling angle and saturating field.[8] The experimentally determined coupling angles $2\Delta\gamma$ and saturating fields H_S are related to the interlayer exchange energies J_1 and J_2 via the areal energy density E of the system in an external field H under the assumption of a negligible in-plane anisotropy[32]

$$E = -M_S d_{FM} H \cos(\Delta\gamma) - J_1 \cos(2\Delta\gamma) + J_2 \cos^2(2\Delta\gamma). \tag{7}$$

The assumption of a negligible in-plane anisotropy can be justified by taking into account the gradual rotation of the magnetization vector and absence of domain wall movement with increasing field or temperature. In Eq. (7) J_1 and J_2 represent the bilinear and biquadratic interlayer exchange coupling energies of the multilayer with volume magnetization density M_S and ferromagnetic layer thickness d_{FM}. Application of an energy minimization procedure leads to two conditions for the interlayer exchange energies. At low fields, $H \sim 0$, the first derivative condition, $dE/d2\Delta\gamma|_{H=0} = 0$, yields

$$\cos(2\Delta\gamma)|_{H=0} = \frac{J_1}{2J_2}. \tag{8}$$

At the point of saturation, where all layers show FM alignment and the respective angle $2\Delta\gamma = 0$, one obtains

$$\tfrac{1}{4} M_S d_{FM} H = 2J_2 - J_1 \tag{9}$$

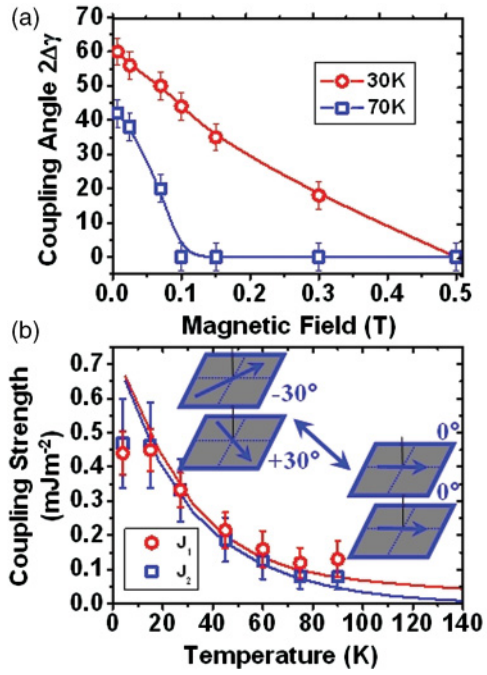

FIG. 9. (Color online) (a) Field dependence of the coupling angle $2\Delta\gamma$ in the sample with 19 Å $Cu_{0.94}Mn_{0.06}$ (lines are a guide to the eye). (b) Temperature dependence of J_1 and J_2 reproduced from.[8] The lines in (b) are fits obtained from the model reported by Saerbeck *et al.*[8]

from the second derivative ($d^2E/d2\Delta\gamma^2|_{2\Delta\gamma=0} > 0$). M_S and d_{FM} in saturated and multidomain states follow directly from fits of the specular PNR data. Furthermore, the PNR simulation presented indicates a homogeneous behavior of the sample (i.e., no large domain formations are present, which would have to be accounted for by two or more different areal energy densities). Therefore, PNR uniquely determines the magnetic energy of the multilayer in every state of domain formation and canting. The resulting bilinear,

$$J_1 = \frac{M_S d_{FM} H_S \cos(2\Delta\gamma)}{4[1-\cos(2\Delta\gamma)]}, \tag{10}$$

and biquadratic interlayer exchange energy,

$$J_2 = \frac{M_S d_{FM} H_S}{8[1-\cos(2\Delta\gamma)]}, \tag{11}$$

are shown in Fig. 9(b). A theoretical approach can now be made by computing exchange energies of different physical origins and comparison made to the experiment.

The lines in Fig. 9(b) represent fits to the data that have been obtained via a model based on a loose spin coupling formalism.[8] As we have shown, the behavior of the magnetic structure in $Cu_{0.94}Mn_{0.06}$/Co multilayers can be well explained by additionally taking into account lateral fluctuations in the Mn impurity density. Such fluctuations lead to a lateral varying loose spin coupling, which induces an additional biquadratic energy contribution via the fluctuation mechanism.[33]

V. CONCLUSION

In conclusion, we have investigated the effect of dilute magnetic Mn impurities on the magnetic behavior of a Co/Cu multilayer system by polarized neutron reflectometry. Analysis of specular and off-specular scattering profiles provides a very detailed model of the temperature and external magnetic field dependent interlayer exchange coupling in the $Cu_{0.94}Mn_{0.06}$/Co multilayers. The parameter set obtained from the simulations is complete in that it is sufficient to describe the magnetization of the system in the low-temperature canted domain and 300 K ferromagnetic aligned state. The loose spin coupling approach taken in Saerbeck *et al.*[8] reproduces our observations well. Additional PNR measurements, taken on different $Cu_{0.94}Mn_{0.06}$ spacer layer thicknesses, show a consistent magnetic structure and support the theoretical approach. This highlights that the canted magnetic structure is a phenomenon of greater generality rather than a case of well-matched coupling terms for a single spacer thickness. Combined PNR and theoretical analysis of the system as a function of Mn impurity concentration will further test the theory and determine the impact of dilute magnetic impurities on the interlayer exchange coupling of the host system.

Our analysis highlights the unique capability of PNR in determination of depth-resolved magnetization profiles in magnetic multilayers. Accurate measures of complicated 2D domain states, coupled with high vertical correlation through the multilayer, are obtained and individual coupling angles determined at distinct external field and temperature values. Structural and averaged bulk magnetizations integrated over the sample are obtained simultaneously and allow conclusions about the large-scale homogeneity of the sample. Together with supporting measurements of complementary techniques, such as magnetometry and x-ray reflectometry, unambiguous 3D layer resolved vector models can be obtained, which is a unique characteristic of PNR.

ACKNOWLEDGMENTS

We acknowledge financial support from the Access to Major Research Facilities Programme and the Australian Research Council (ARC).

*thomas.saerbeck@ansto.gov.au

[1] S. D. Bader and S. S. P. Parkin, Annu. Rev. Condens. Matter Phys. **1**, 71 (2010).

[2] S. S. P. Parkin, C. Kaiser, A. Panchula, P. M. Rice, B. Hughes, M. Samant, and S.-H. Yang, Nature Mater. **3**, 862 (2004).

[3] D. M. Edwards and A. Umerski, in *Handbook of Magnetism and Advanced Magnetic Materials*, edited by H. Kronmueller and S. Parkin, Vol. 1 (Wiley, New York, 2007), p. 487.

[4] *Ultrathin Magnetic Structures*, edited by B. Heinrich and J. A. C. Bland, Vols. 2 and 3 (Springer, Berlin, 1994 and 2005).

[5] P. Grünberg, Ann. Phys. **17**, 7 (2008).

[6] *Magnetic Heterostructures*, edited by H. Zabel and S. D. Bader, STMP 227 (Springer, Berlin, 2008)

[7] Y. Kobayashi, Y. Aoki, H. Sato, R. Loloee, and W. P. Pratt Jr., Phys. Rev. B **59**, 3734 (1999).

[8]T. Saerbeck, N. Loh, D. Lott, B. P. Toperverg, A. M. Mulders, A. F. Rodriguez, J. W. Freeland, M. Ali, B. J. Hickey, A. P. J. Stampfl, F. Klose, and R. L. Stamps, Phys. Rev. Lett. **107**, 127201 (2011).

[9]C. H. Marrows, L. C. Chapon, and S. Langridge, Mater. Today **12**, 70 (2009).

[10]B. P. Toperverg (unpublished). The software for fitting PNR data and simulating off-specular neutron scattering is available from: Boris.Toperverg@RUB.de, or boris@ill.fr.

[11]H. Zabel, K. Theis-Bröhl, and B. P. Toperverg, in *Handbook of Magnetism and Advanced Magnetic Materials*, edited by H. Kronmueller and S. S. P. Parkin, Vol. 3 (Wiley, New York, 2007), p. 1237.

[12]D. Solina, D. Lott, U. Tietze, O. Frank, V. Leiner, and A. Schreyer, Physica B: Cond. Matt. **385–386**, 1167 (2006).

[13]V. G. Syromyatnikov, A. F. Schebetov, D. Lott, A. P. Bulkin, N. K. Pleshanov, and V. M. Pusenkov, Nucl. Instrum. Methods Phys. Res., Sect. A **634**, S126 (2011).

[14]M. R. Fitzsimmons, S. D. Bader, J. A. Borchers, G. P. Felcher, J. K. Furdyna, A. Hoffmann, J. B. Kortright, I. K. Schuller, T. C. Schulthess, S. K. Sinha, M. F. Toney, D. Weller, and S. Wolf, J. Magn. Magn. Mater. **271**, 103 (2004).

[15]C. F. Majkrzak, N. F. Berk, and K. V. O'Donovan, in *Neutron Scattering From Magnetic Materials*, edited by T. K. Chaterji (Elsevier, Amsterdam, 2005).

[16]A. Ney, P. Poulopoulos, and K. Baberschke, Europhys. Lett. **54**, 820 (2001).

[17]Simulations have been performed using the SUPREX. program: E. Fullerton, Ivan K. Schuller, H. Vanderstraeten, and Y. Bruynseraede, Phys. Rev. B **45**, 9292 (1992); D. M. Kelly, E. E. Fullerton, J. Santamaria, and I. K. Schuller, Scr. Metall. Mater. **33**, 1603 (1995).

[18]P. Scherrer, Nachr. Ges. Wiss. Göttingen **26**, 98 (1918).

[19]J. I. Langford and A. J. C. Wilson, J. Appl. Crystallogr. **11**, 102 (1978).

[20]Program and description available from http://www.llb.cea.fr/prism/programs/simulreflec/simulreflec.html.

[21]V. Lauter-Pasyuk, H. J. Lauter, B. P. Toperverg, L. Romashev, and V. Ustinov, Phys. Rev. Lett. **89**, 167203 (2002).

[22]B. P. Toperverg, Physica B: Cond. Matt. **297**, 160 (2001).

[23]B. P. Toperverg, O. Nikonov, V. Lauter-Pasyuk, and H. J. Lauter, Physica B **297**, 169 (2001).

[24]B. P. Toperverg, A. Rühm, W. Donner, and H. Dosch, Physica B **267-268**, 198 (1999).

[25]S. K. Sinha, E. B. Sirota, S. Garoff, and H. B. Stanley, Phys. Rev. B **38**, 2297 (1988).

[26]A. Rühm, B. P. Toperverg, and H. Dosch, Phys. Rev. B **60**, 16073 (1999).

[27]E. Kentzinger, U. Rücker, B. Toperverg, F. Ott, and T. Brückel, Phys. Rev. B **77**, 104435 (2008).

[28]D. E. Savage, J. Kleiner, N. Schimke, Y. H. Phang, T. Jankowski, J. Jacobs, R. Kariotis, and M. G. Lagally, J. Appl. Phys. **69**, 1411 (1991).

[29]O. Glatter, O. Kratky, *Small Angle X-ray Scattering* (Academic Press, London, 1982).

[30]S. K. Sinha, Mater. Res. Soc. Symp. Proc. **376**, 175 (1995).

[31]S. Langridge, J. Schmalian, C. H. Marrows, D. T. Dekadjevi, and B. J. Hickey, Phys. Rev. Lett. **85**, 4964 (2000).

[32]F. Schreiber, A. Soliman, P. Bödeker, R. Meckenstock, K. Bröhl, and J. Pelzl, J. Magn. Magn. Mater. **135**, 215 (1994).

[33]J. C. Slonczewski, J. Magn. Magn. Mater. **150**, 13 (1995).